Numerical models for planar solid oxide fuel cells

Beale, Steven

Publisher's version / Version de l'éditeur:

Transport Phenomena in Fuel Cells, pp. 43-82, 2005

CHAPTER 2

Numerical models for planar solid oxide fuel cells

S.B. Beale
National Research Council, Ottawa, Canada.

Abstract

This article discusses various numerical techniques used to model single-cells and stacks of planar solid oxide fuel cells. A brief history of the solid oxide fuel cell (SOFC), and a survey of modeling efforts to-date are presented. The fundamental thermodynamics of the SOFC are introduced, together with the equations governing the ideal (Nernst) potential. Factors affecting operating cell voltages are then discussed. A simple iterative calculation procedure is described, whereby inlet mass factions, flow rates, and cell voltage are known, but outlet values, and current are required. This provides a paradigm for more complex algorithms set out in the remainder of the text. The next level of complexity is provided for by numerical integration schemes based on 'presumed-flow' methodologies, where the inlet flow rates of oxidant and fuel are assumed to be uniform. Local mass sources and sinks are computed from Faraday's equation. These are then used to correct the continuity and mass transfer equations. Temperature variations are also computed; because heat and mass transfer effects affect the output of SOFCs, significantly. Some more advanced chemistry, heat and mass transfer issues are further detailed. The most detailed cell models are obtained using computational fluid dynamics codes, based on finite-volume and other techniques. Additional improvements to these (and other) codes involve the detailed modeling of the electric potential (in place of the Nernst equation formulation), and the analysis of the combined kinetics and mass transfer problem in the porous electrode media. Finally stack models are introduced. These may be full-scale computational fluid dynamics models or simpler models based on volume-averaging techniques.

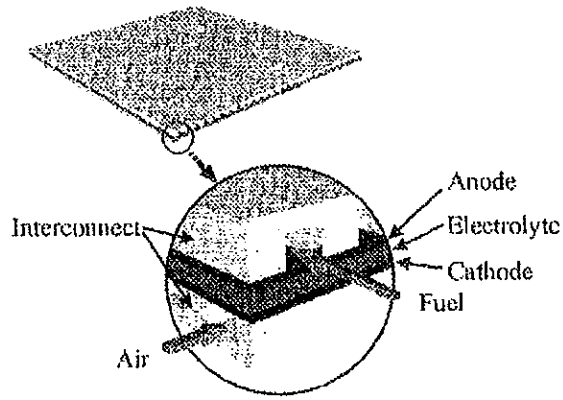

Figure 1: Schematic of typical planar SOFC.

1 Introduction

1.1 History and types of solid oxide fuel cell

There are many types of fuel cell under development. Most popular among these are the proton exchange membrane fuel cell (PEMFC) and the solid oxide fuel cell (SOFC) [1–3]. The SOFC is a solid-state device that utilizes the oxygen ion conducting property of the ceramic zirconia. The operation of a SOFC differs from that of a PEMFC or a conventional battery, in that both electronic and ionic circuits are due to the flux of negatively charged particles; electrons and O^{2-} ions. The positive ions or 'holes' are immobilised in the solid matrix, at the time of fabrication. The book by Williams [4] details developments in SOFC technology prior to the 1960's.

A SOFC consists of an *anode* or fuel electrode, an *electrolyte*, and a *cathode* or air electrode. The anode is typically a porous cermet, for example the combination of NiO and Yttria-stabilised Zirconia (YSZ). A typical material for the cathode is Sr doped $LaMnO_3$, a perovskite. The electrolyte consists of a layer of YSZ, and is fabricated as thin as possible in order to reduce Ohmic losses. *Fuel and air passages* are required to supply the products and remove the reactants; the gas passages are typically rectangular micro-channels, though planar channels may also be utilized occasionally. In addition, porous media inserted between the fluid passages and electrodes may serve as *gas diffusion layers*.

Both planar and cylindrical SOFC geometries are to be found; the latter avoid mechanical sealing problems, whereas the former allow for relatively large electrical power densities to be achieved. The discussion in this paper focuses on the planar design. In order to reach the necessary operating voltage, fuel cells are connected together in a *stack* by situating a metallic or ceramic *interconnect* between each cell. These are often made of stainless steel. Cells are connected electrically

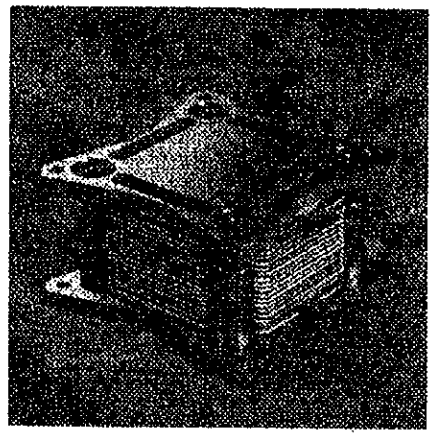

Figure 2: Planar SOFC stack. Courtesy Global Thermoelectric Inc.

in series, but hydraulically in parallel. The interconnects also function as a housing for the flow channels for the air and fuel which are supplied via manifolds. The balance-of-plant makes sure that the working fluids are supplied under the desired operating conditions. Fuel cells may be operated in co-flow, counter-flow and cross-flow. The industrial SOFC designs encountered by the present author were for cross-flow. Hydrogen is normally provided by reforming methane or methanol in a reactor. The electrical efficiency of a system running on natural gas can exceed 50%. The remaining energy is released as heat.

The basic operation of a SOFC is as follows: reduction takes place at the cathode.

$$O_2 + 4e^- \rightarrow 2O^{2-}. \tag{1}$$

At the anode, if the fuel is H_2, the oxygen ion combines with hydrogen to form water, electricity and heat.

$$H_2 + O^{2-} \rightarrow H_2O + 2e^-. \tag{2}$$

Thus the overall reaction is

$$\begin{gathered} H_2 + \tfrac{1}{2}O_2 \rightarrow H_2O. \\ 1\,\text{kg} + 8\,\text{kg} \qquad 9\,\text{kg} \end{gathered} \tag{3}$$

1.2 Survey of modeling techniques

Mathematical models of heat and mass transfer and electrochemistry provide tools for performance prediction of single-cells and stacks of fuel cells. Thermo-fluid simulations can predict the thermal and electrochemical performance, and structural analysis models can predict the mechanical behavior. Our concern here is

with the former. Among the first to perform calculations on SOFC performance were Vayenas and Hegedus [5]. Since then, the scope and detail of modeling have increased. Models have been developed at various scales: micro-scale or nano-scale studies aim at the development of better electrodes through mathematical analysis. Single-cell models are often the first consideration for fuel cell manufacturers embarking on a new product design, and are currently a target application for the vendors of commercial CFD codes. Stack modeling is necessary for the overall design and often involves parametric studies. Among the most salient issues that need to be addressed are the electric potential field, porous media transport phenomena, and chemical kinetics (shift reactions, internal reforming). The development of a model for conservation of heat, mass, and charge in SOFCs is detailed in [6–8]. Such models have been applied to SOFC stacks [9–12]. Shift and reforming reactions have also been considered [13, 14] as well as heat and mass transfer issues [15, 16]. The size and complexity of SOFC stacks requires the use of very large computers, if a conventional CFD code is employed. Because of this, simpler models based on engineering assumptions have sometimes been devised [10, 12, 17, 18] in order that personal computers may perform such calculations. The speed and memory requirements of a computer code will be limited by the application. For detailed SOFC design large-scale CFD codes will be required, whereas for real-time control, rapid response will preclude all but the simplest of schemes from being employed.

1.3 Thermodynamics of solid oxide fuel cells

Newman [19] states that thermodynamics, kinetics, and transport phenomena are fundamental to understanding electrochemical systems. It is important to realise that transport phenomena are affected by thermodynamic properties and chemical kinetics. Physicochemical hydrodynamics [20, 21] is the study of such mutual interactions. It is timely to start with the thermodynamics of fuel cells. Figure 3 illustrates the notion of the fuel cell as a thermodynamic device. It is postulated

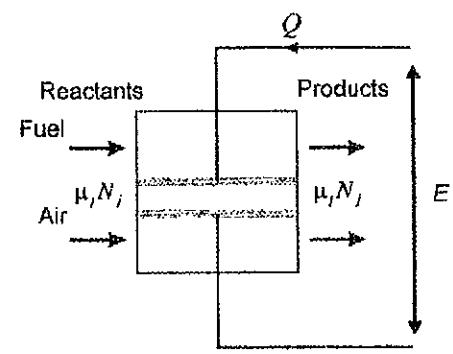

Figure 3: Fuel cell as a thermodynamic system.

that the fundamental relation [22] for the internal energy, U, may be expressed as

$$U = U(S, V, N_j, Q), \tag{4}$$

where S is entropy, V is volume, N_j is mole number of species j, and Q is charge number. Conservation of energy requires that,

$$dU = dW_{\text{Heat}} + dW_{\text{Mech}} + dW_{\text{Chem}} + dW_{\text{Elec}}, \tag{5}$$

$$dU = TdS - PdV + \sum_j \mu_j dN_j + EdQ, \tag{6}$$

where $T = (\partial U/\partial S)_{V,N_j,Q}$, $P = -(\partial U/\partial V)_{S,N_j,Q}$, $\mu_j = (\partial U/\partial N_i)_{S,V,Q}$, and $E = (\partial U/\partial Q)_{S,V,N_j}$ are temperature, pressure, chemical potential, and electric potential, respectively.

Texts in physical chemistry invariably introduce Gibbs free energy, G, which for a chemical reaction which does not involve charge transfer may be written:

$$dG = dU - TdS + PdV = \sum_j \mu_j dN_j. \tag{7}$$

The free energy is useful for analysis of situations where temperature and pressure are constant (e.g. at ambient). Note that for the situation under consideration $dU - TdS + PdV \neq \sum_j \mu_j dN_j$.

For an electrochemical process, where temperature and pressure are maintained constant and there is no change in internal energy, chemical energy is converted to electrical energy:

$$\sum_j \mu_j dN_j = -EdQ, \tag{8}$$

where it is understood that N_j is positive for inflow and negative for outflow, i.e., the sum of chemical energy of the reactants less that of the products.

The molar enthalpy of formation of the chemical reaction defined by eqn (3) is $\Delta H^0 = -247.3$ kJ/mol at 1000 °C, whereas the molar Gibbs energy of formation (i.e. the chemical energy of formation) is $\Delta G^0 = -177.4$ kJ/mol, the negative sign indicating that heat will be released at a rate of 69.9 kJ/mol. The electrochemical reaction is thus exothermic. The difference between these terms $\Delta H^0 - \Delta G^0$ is frequently referred to in a somewhat cavalier fashion as the $T\Delta S^0$ term. However there are other heat sources in a fuel cell, which can change the entropy (and internal energy) of the system. It is also worth noting that a fuel cell is not open to the atmosphere, so pressure and temperature can and do vary. It is therefore prudent to appreciate that eqn (8) is just a simplified form of eqn (6). Nonetheless it is eqn (8) that is invariably the point of departure for a fuel cell analysis, with irreversibilities being added to modify the basic postulate that ideally all chemical energy would be converted to electrical energy.

Since the air and fuel in a SOFC are high-temperature gases, we may treat them as multi-component perfect gases, such that

$$PV = NRT, \tag{9}$$

where $R = 8.3144 \times 10^3$ J/mol.K is the gas constant, and

$$N = \sum_j N_j \tag{10}$$

for the air-side and fuel-side gases. The chemical potentials are given by [22]:

$$\mu_j = \mu_j^0(T) + RT \ln P + RT \ln x_j = \mu_j^0(T) + RT \ln P_j, \tag{11}$$

where

$$x_j = N_j/N = N_j \Big/ \sum_k N_k \tag{12}$$

is mole fraction and $P_j = x_j P$ is the partial pressure of species j.

Faraday's law gives the number of moles of oxygen consumed by the electrochemical reaction as

$$\tilde{N} = \frac{Q}{nF}, \tag{13}$$

where $F = 96\,485$ Coulomb/mol is Faraday's constant and $n = 2$ is the valence of oxygen.

Thus the change in chemical energy is

$$\sum \mu_j \Delta N_j = \sum \left[(\nu_j \mu_j)_{\text{Products}} - (\nu_j \mu_j)_{\text{Reactants}} \right] \tilde{N} \tag{14}$$

and ν_i are stoichiometric coefficients. For example,

$$\nu_1 A_1 + \nu_2 A_2 \rightarrow \nu_3 A_3, \tag{15}$$

$$\sum \mu_i \Delta N_i = (\nu_1 \mu_1 + \nu_2 \mu_2 - \nu_3 \mu_3)\tilde{N} = (\Delta G^0 + RT \ln K_p)\tilde{N}, \tag{16}$$

where $\Delta G^0 = \sum [(\nu_j \mu_j)_{\text{Products}} - (\nu_j \mu_j)_{\text{Reactants}}]$ is referred to as the molar Gibbs free energy for the chemical reaction. (NB: The author denotes $\Delta G = G/\tilde{N}$ J/mol for consistency with the literature).

The equilibrium constant, K_P, is given by

$$K_p = \frac{P_1^{\nu_1} P_2^{\nu_2}}{P_3^{\nu_3}}. \tag{17}$$

This may be re-written in terms of mole fractions, x_j, e.g., for a SOFC with hydrogen as fuel:

$$\sum \mu_i \Delta N_i = \left(\Delta G^0 + \frac{1}{2} RT \ln P_a + RT \ln \left(\frac{x_{H_2} x_{O_2}^{0.5}}{x_{H_2O}} \right) \right) \tilde{N}, \tag{18}$$

where P_a is air pressure. Substituting molar flow rate for current using Faraday's law we immediately obtain

$$E = -\frac{\sum \mu_j \Delta N_j}{nF}. \tag{19}$$

Since the valence of oxygen is 2, we have,

$$E = E^0 + \frac{RT}{2F} \ln \left(\frac{x_{H_2} x_{O_2}^{0.5}}{x_{H_2O}} \right) + \frac{RT}{4F} \ln P_a \tag{20}$$

which is the *Nernst equation* for a solid oxide fuel cell. The quantity E is the reversible or *Nernst potential*. In what follows below, we make the assumption that we may associate the thermodynamic pressure with the hydrodynamic pressure, and the thermodynamic potential with the electrostatic potential. For practical reasons, E^0 is redefined such that P_a is gauge (relative) pressure rather than absolute air pressure, in which case the latter term in eqn (20) is replaced by the form $(RT/4F) \ln (1+P_{gauge}/P_0)$, and P_0 is a reference operating pressure. The latter form is more useful when considering detailed transport models where values of pressure and temperature vary. Generally speaking P_{gauge}/P_0 is very small so changes in E are largely due to variations in mole fraction and temperature.

Values of E^0 are typically enumerated as polynomials, e.g.,

$$E^0 = a - bT. \tag{21}$$

Typical values would be $a = 1.214$ V and $b = 3.2668$ V/K. Higher order polynomials may also be found. The physical significance of the terms on the right-side of eqn (21) are $a \approx \Delta G^0/nF$ and $b \approx T\Delta S^0/nF$. Although these terms are themselves temperature dependent, this is a quite reasonable approximation in many situations. The process illustrated in Fig. 3 is an open thermodynamic cycle. Thus when a load is connected, a finite current $i = \dot{Q}$ flows. Under these circumstances there will be irreversible changes, and the actual cell voltage will be lower than the reversible Nernst potential.

1.4 Cell voltage and current

The conduction mechanism in the ionic electrolyte differs fundamentally from that in the neighbouring electrodes and interconnects (electronic conduction). Therefore the electrolyte *polarises* at the edges and a *double charge layer* is established at the interfaces. The change in chemical potential across the interface, $\Delta\mu_j$, is balanced by the opposing change in the electric potential for electrochemical equilibrium, $nF\Delta\phi$. The sum of these terms is referred to as the electrochemical potential. Figure 4 illustrates the double charge layer in a fuel cell, while Fig. 5 shows the potential distribution. The Nernst potential is just the sum of the anodic and cathodic potentials, $E = \Delta\phi_a + \Delta\phi_c$. It is not possible to measure the potential, $\Delta\phi$, at a single electrode, though it is possible to measure changes from equilibrium, $\eta = \delta\Delta\phi$,

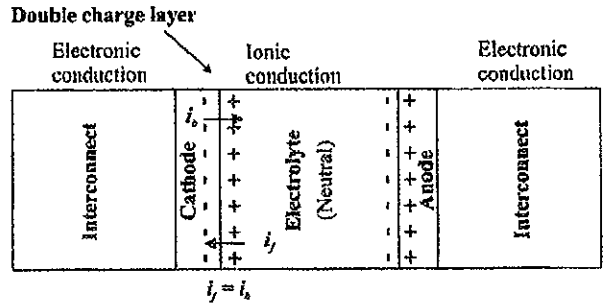

Figure 4: Double charge layer.

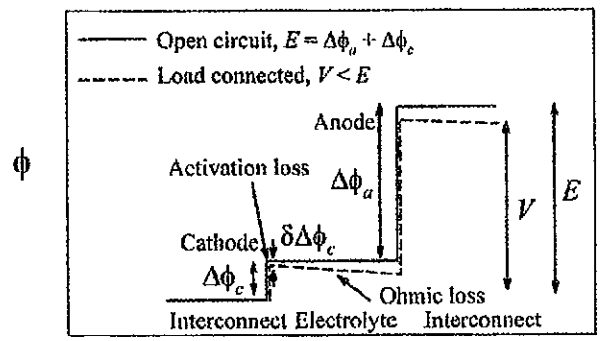

Figure 5: Electric potential at open circuit and with a current flowing.

when a current is drawn. The double-layer is just a few nanometres thick. There is no net change in potential, in the absence of an electric current, within the bulk of the electrolyte. In other words, there are step changes in potential at the anode and the cathode, but zero change within the electrolyte, as shown in Fig. 5.

Whenever a current, i, is drawn, the voltage drops and the actual *cell voltage*, V, is given by

$$V = E - \eta_e - \eta_a - \eta_c = iR_l, \tag{22}$$

where the terms η_e, η_a and η_c are electrolytic, anodic, and cathodic losses, respectively. These have often been referred to as *overpotentials* or *polarisations* in the electrochemistry and chemical engineering literature. R_l is the resistance of the external load.

The potential difference across the electrolyte

$$\eta_e = iR_e = E - \eta_a - \eta_c - V \tag{23}$$

is sometimes referred to as the Ohmic overpotential. Here R_e is the internal resistance of the electrolyte. The resistivity of the electrolyte is highly temperature dependent, and decreases with increasing temperature. There will also be a similar (usually smaller) Ohmic loss associated with metallic interconnect(s), and for

convenience that latter will be ignored for now. Thus work is being done by the electric field on the ions in the electrolyte and interconnects, whereas work is being done against the field in crossing the electrodes. Although the anodic and cathodic overpotentials are themselves a function of the current, it is sometimes convenient for numerical purposes to lump all the losses into a single linearised internal resistance, $\bar{R}$

$$\eta_e + \eta_a + \eta_c = i\bar{R}, \tag{24}$$

where it is understood that $\bar{R} = \bar{R}(i)$, i.e. the slope of the *V-i* curve is not constant. The *V-i* curve or, more often the voltage-current-density, *V-i''*, curve is the single most important characteristic to the electrochemical scientist. N.B. The reader will note that in this text, a 'dot' is used to denote a time derivative, and a 'dash' to denote a length derivative. Thus if q has units [J], then $\dot{q}''$ has units [W/m^2].

While mole fractions are often found in electrochemical texts, in engineering problems it is much more common to utilize mass fractions, m_j, which may be converted to/from molar fractions, x_j, as follows:

$$m_j = x_j \frac{M_j}{M}, \tag{25}$$

where the mixture molecular weight is just

$$M = \sum_j x_j M_j = \frac{1}{\sum_j \frac{m_j}{M_j}}. \tag{26}$$

The reactions at the electrode surfaces lead to continuity and species sources/sinks in the working fluids. The mass fluxes, $\dot{m}_j''$ (in kg/m^{2}s), are related to the current density, $i'' = i/A$, by Faraday's law

$$\dot{m}_j'' = \pm \frac{M_j i''}{1000 n_j F}, \tag{27}$$

where M_j is the molecular weight of chemical species j (in g/mol), and n is the valence. It is trivial to re-write the Nernst equation in terms of mass fractions.

$$E = E^0 + \frac{RT}{2F}\left[\ln\left(\frac{m_{H_2} m_{O_2}^{0.5}}{m_{H_2O}}\right) + \frac{1}{2}\ln(M_a) + 0.4643\right] + \frac{RT}{4F}\ln P_a, \tag{28}$$

where M_a is the mixture molecular weight, eqn (26), for air, and

$$\ln\left(\frac{M_{H_2O}}{M_{H_2} M_{O_2}^{0.5}}\right) \approx \ln(18) - \ln(2) - \tfrac{1}{2}\ln(32) = 0.4643. \tag{29}$$

In electrochemistry, molar-based units are frequently encountered, but in transport phenomena, for a variety of reasons, mass-based units are preferred. This duality is a fact-of-life when dealing with fuel cells. Both have their uses and limitations.

1.5 Activation losses

Electrochemical reactions can only occur at finite rates. For a charged particle to pass across a double charge layer, it must possess more free energy than a certain minimum. From an engineering perspective the activation energy is similar to bulk-to-interphase energy, required for example in multi-phase systems involving phase-change. Figure 6 illustrates the basic principle for a single-step single-electron electrochemical reaction $A \rightarrow B$. The sharp sign, #, indicates the activated state. Eyring's analysis [23] is useful for such rate-limiting situations. The analysis proceeds as follows: the probability density function for ions crossing the electrode boundary follows a Boltzmann distribution, and it can readily be shown that the forward *rate constant*, k_f mol/sec, is given by

$$k_f = k_0 \exp(-\Delta G_f / RT). \tag{30}$$

A backward rate constant, k_b, is similarly defined. For an open circuit (equilibrium), $k_f = k_b = k_0$. If a current flows, the potential difference deviates from the open circuit value, and the required free energy will also change as a result of the electric field:

$$\Delta G = \Delta G_f - \beta F \Delta\phi, \tag{31}$$

where β is a symmetry coefficient, $0 \leq \beta \leq 1$, which is a measure by which a change in electric potential affects the required activation energy, see Fig. 6. Under this condition, the forward rate will not equal the backward rate. The former is given by,

$$i_f = F N_A k_0 \exp(-\Delta G_f / RT) \exp(-\eta F \Delta\phi / RT) = i_0 \exp(-\beta F \eta / RT), \tag{32}$$

where x_A is the mole fraction of compound A, and M is the mixture molecular weight. The quantity $\eta = \delta\Delta\phi = \Delta\phi - \Delta\phi_0$ is the so-called *activation overpotential*. Similarly, for the backwards reaction $B \rightarrow A$ the charge flux of charge is

$$i_b = i_0 \exp(-(1-\beta) F \eta / RT) \tag{33}$$

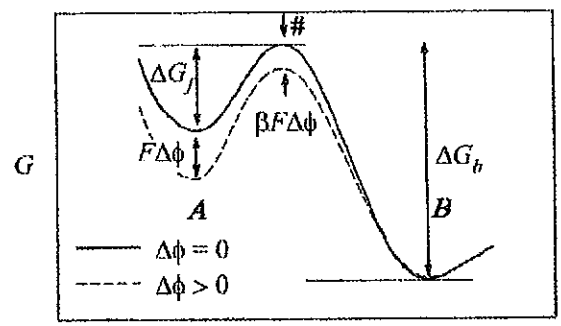

Figure 6: Schematic of concept of activation energy for a single-step single-electron transfer reaction.

and the form of the *Butler-Volmer equation*, appropriate for a single-step single-electron transfer process, is obtained,

$$i = i_0[\exp(-\beta nF\eta/RT) - \exp((1-\beta)nF\eta/RT)]. \quad (34)$$

The quantity i_0 is the *exchange current*. In general i_0 will be a function of molar concentration. That dependence can be theoretically determined by ensuring compatibility with the thermodynamic requirement $E = E^0 + (RT/F)\log(P_B/P_A)$ for equilibrium, where P_A and P_B are partial pressures. Setting $i_f = i_b = i_0$ it follows that the exchange current density is just $i_0'' = Fk_0P_A^{1-\beta}P_B^{\beta}$.

The two terms in eqn (34) are essentially similar to Arrhenius-type expressions occurring in chemically reacting systems. The following points are noted: for small currents, eqn (34) reduces to a linear form, obtained by expanding it in a Taylor series about $\eta = 0$. At higher overpotentials (currents) an exponential form is obtained; for the latter situation one of the two terms in eqn (34) is negligibly small, depending on the direction of flux of charged particles. The exponential form is referred to as a *Tafel equation*. The ratio i/i_0 determines if one is in the linear or Tafel regions. For a multi-step electrochemical reaction, the Butler-Volmer equation is generally written,

$$i = i_0[\exp(n\beta_f F\eta/RT) - \exp(-n\beta_b F\eta/RT)]. \quad (35)$$

The quantities β_f and β_b are referred to as *transfer coefficients*. In deriving eqn (35) for a multi-step reaction [24, 25] it is generally assumed that at any electrode there is only one *rate limiting step*, with all other steps being considered at equilibrium. In view of these restrictions, it is probably wise to regard eqn (35) as being a semi-empirical formulation, for which β_f and β_b are determined experimentally. Equation (35) may be considered as an implicit form of the relationship of $\eta = \eta(i, T)$ which must be solved iteratively, for any given i_0 and β. Typical values for planar SOFCs are $i_0'' = 1 - 5\,000\ \mathrm{A/m^2}$. In general two sets of eqn (35) must be solved at both the anode and cathode to yield η_a and η_c for use in eqn (22), i.e. there are two values of i_0'' and four of β (N.B. β is often assumed to be ½). The overpotential at one electrode may be negligible compared to the other. Following the argument above for a single-step reaction for two electrodes, and imposing the requirement that for equilibrium, the sum of the potentials must equal the thermodynamic Nernst potential, eqn (20), and with the additional assumption that $\beta_f = \beta_b = 1/2$, it may be reasonably concluded that the concentration dependence of the exchange current is $i_0 \propto P_{O_2}^{0.25}$ at the cathode and $i_0 \propto P_{H_2}^{0.5}P_{H_2O}^{0.5}$ at the anode for a SOFC.

Simplifying the Butler-Volmer equation has the advantage of rendering an explicit solution for $\eta(i, T)$; however the calculation procedure for the cell/stack is iterative by nature, and therefore there is little problem in using the implicit form, above. Charge transfer losses are particularly important at low current densities. The SOFC is a high-temperature device, and thus activation losses are generally less significant than in other fuel cells such as proton exchange membrane fuel cells, due to the presence of the exponent $(RT)^{-1}$. The subject of electrode kinetics, or electrodics, is an important one and the reader interested in more than the brief overview

provided here is referred to specialised texts such as Gileadi [24], Bockris *et al.* [25] and Bard and Falkner [26].

1.6 Diffusion losses

Mass transfer losses are due to diffusion becoming a rate limiting factor in providing O_2 and H_2 to the cathode and anode, and removing H_2O at the anode. Thus transport phenomena in the fuel and air channels can and do affect the electrical performance of the fuel cell. This becomes increasingly important at high current densities where concentration gradients are high. Mass transfer effects are sometimes handled in an analogous manner to charge transfer (activation) by introducing a *concentration overpotential*, also known as a *concentration polarisation*. The origin of these terms is historical. They may be written in terms of either molar or mass fractions. The latter is adopted here, namely

$$\eta = \pm\frac{RT}{nF}\ln\left(\frac{m_b}{m_w}\right) \tag{36}$$

for inclusion in eqn (22). The symbols m_b and m_w denote bulk and wall values of mass fraction (in the interests of readability the indicial notation $m_{j,b}$ etc., is dropped) and the sign is positive for products and negative for reactants. There is no real advantage to defining overpotentials in the form of eqn (22). Rather, all that is necessary is the recognition that the Nernst equation be based on wall values, instead of those in the bulk of the fluid. Some authors [3, 27] suggest that diffusion effects in fuel cells be modelled using so-called equivalent film theory, introducing a Nernst length scale. That approach is not recommended here. The suggested approach for mass transfer calculations in SOFCs is outlined in Beale [28] and follows standard approaches [29–32] to the generalized engineering mass transfer problem.

In fuel cells, heterogeneous chemical reactions on the electrode surfaces lead to sources and sinks in the continuity and species (mass fraction) equations. Let it be supposed that the mass flux, $\dot{m}''$, is given by

$$\dot{m}'' = gB, \tag{37}$$

where $\dot{m}'' = \pm M i''/1000nF$ is negative for O_2 and H_2 and positive for H_2O, and g is a mass transfer *conductance*. For historical reasons the symbol g is used to represent a generalised conductance, whereas the symbols h (Europe) and α (N. America) are reserved for heat transfer, with temperature as independent variable. There is clearly an element of redundancy in this convention.

The *driving force*, B, is defined by

$$B = \frac{m_b - m_w}{m_w - m_f}. \tag{38}$$

By convention, both $\dot{m}''$ and B are positive for injection (H_2O at the anode) and negative for suction (O_2 and H_2 at the cathode and anode, respectively),

while the conductance g is always positive. The subscript, t, refers to the so-called *transferred-substance state* (T-state) [29, 32, 33]. For multi-component mixtures, T-state values are given by,

$$m_{j,t} = \frac{\dot{m}''_j}{\dot{m}''}, \tag{39}$$

where $\dot{m}'' = \sum_j \dot{m}''_j$. Thus it can be seen from the stoichiometry of eqn (3) that for the air-side $m_t = 1$ for O_2, whereas $m_t = -1/8$ for H_2 and $m_t = +9/8$ for H_2O on the fuel-side. Equation (37) may be conveniently rewritten in dimensionless form

$$B = \frac{g^*}{g} b, \tag{40}$$

where g^* denotes the value of g in the limit $\dot{m}'' \to 0$, and the blowing parameter, b, is given by

$$b = \frac{\dot{m}''}{g^*}. \tag{41}$$

Equation (38) may be rearranged to obtain the required form

$$\frac{m_w}{m_b} = \frac{1 + \frac{m_t}{m_b} B}{1 + B}. \tag{42}$$

Ideally actual mass transfer data for $B(b)$ for the particular channel geometry under consideration are available; if not, the solution to the 1-D convection-diffusion equation,

$$B = \exp(b) - 1 \tag{43}$$

may be used as an approximation. Figure 7 shows data from numerical simulations of fully-developed mass transfer in ducts of various geometries [34]. It can be

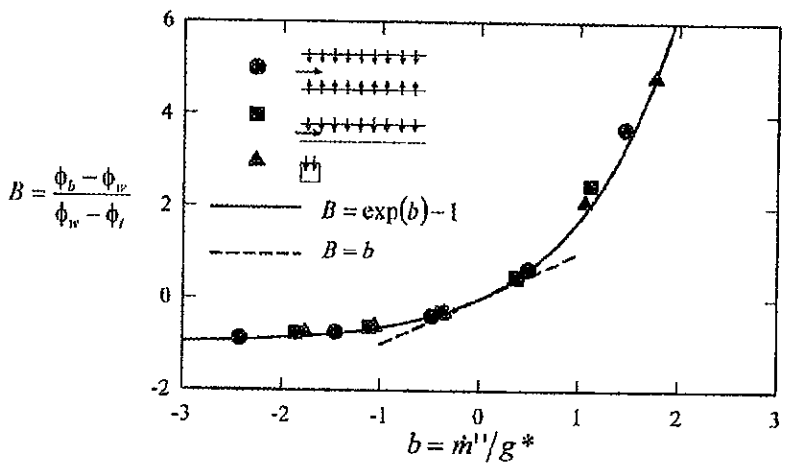

Figure 7: Mass transfer driving force as a function of blowing parameter, from [28].

seen that data normalized in the form of B vs. b (or equivalent) conforms well to the curve corresponding to eqn (43). The choice of non-dimensional number is important; for example use of a wall Reynolds number, Re, or Sherwood number, Sh, for the abscissa in place of the normalised convection flux, b, will not result in the data reducing to (roughly) a single curve. Equations (42) and (43) or equivalent, are sufficient to compute mass transfer losses in the form of eqn (22) in a manner which is reasonably rigorous while at the same time being reasonably simple to implement.

Thus knowledge of g^* for air-side and fuel-side geometries together with experimental data or an analytical expression for $B(b)$ is sufficient to obtain a reasonable estimate of diffusion losses in a fuel cell. Some deviations from Fig. 7 are to be anticipated for a variety of reasons (entry-length considerations, Schmidt number variations, etc.). If experimental data are available, these should always be used. It is to be noted that for many situations the mass flow rates are small, and under the circumstances $g = g^*$ and $B = b$. Values of g^* may be obtained from the zero-mass flux Sherwood number, Sh^*,

$$Sh^* = \frac{g^* D_h}{\Gamma}. \tag{44}$$

Note that diffusion control is important in fuel cells at high current densities/mass fluxes, not in the limit $Sh \to Sh^*$. Figure 8 shows values of Sh^* for fully-developed mass flow and scalar transport in rectangular ducts of various aspect ratios, as given in Table 43 of ref. [35]. It is to be noted that suction (e.g. at the cathode) reduces mass transfer, i.e. $g/g^* < 1$, whereas blowing (e.g. at the anode) has the opposite effect $g/g^* > 1$. Knowledge of the T-state value is also useful when performing detailed CFD simulations. These may be used to prescribe boundary conditions in the species equations (see Section 2.5). Although this introductory analysis is

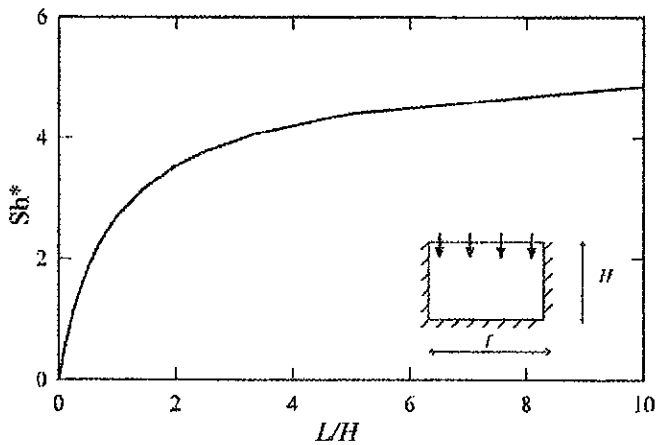

Figure 8: Sh^* (Nu^*) for rectangular ducts in the limit of zero blowing. From [34], data of Schmidt [35].

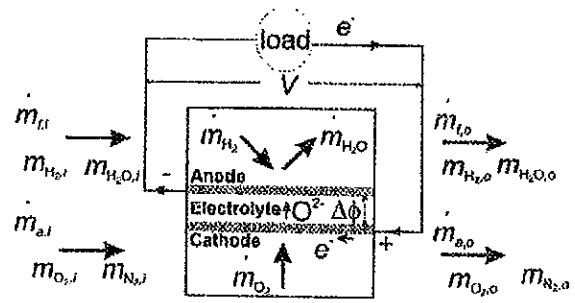

Figure 9: Schematic representation of a SOFC with hydrogen as fuel.

appropriate for mass transfer in the gas channels, Section 2.9 shows that it may be readily extended to consideration of more complex geometries involving combined mass transfer in channels and porous diffusion layers. Section 2.11 discusses some further considerations for mass transfer analysis in fuel cells.

1.7 Basic computational algorithm

We are now in a position to construct a simple algorithm for computation of the performance for a fuel cell. Assume the following are known: cell voltage, V, temperature, T, air pressure P_a, inlet flow rates for air and fuel, $\dot{m}_{a,\text{in}}$, $\dot{m}_{f,\text{in}}$, and mass fractions of the component species in the air, $m_{O_2,\text{in}}$, $m_{N_2,\text{in}}$, and the fuel, $m_{H_2,\text{in}}$, $m_{H_2O,\text{in}}$, respectively.

1. Guess an initial value for the current i.
2. Calculate mass sources/sinks, $\dot{s}_{O_2}$, $\dot{s}_{H_2}$, $\dot{s}_{H_2O}$, from Faraday's law. Compute air and fuel outlet mass flow rates, $\dot{m}_{a,\text{out}}$, $\dot{m}_{f,\text{out}}$, and mass fractions, $m_{O_2,\text{out}}$, $m_{H_2,\text{out}}$, $m_{H_2O,\text{out}}$, $m_{N_2,\text{out}}$.
3. Calculate average of inlet and outlet bulk mass fractions and then compute wall mass fractions, using eqn (42).
4. Compute the anode and cathode overpotentials, η_a, η_c, from the Butler-Volmer equation eqn (35), based on wall values.
5. Compute the Nernst potential, E, from eqn (20), based on wall values.
6. Compute the current, i, from

$$i = \frac{E - \eta_a - \eta_c - V}{R_e}. \tag{45}$$

7. Repeat steps 2–6 until convergence is obtained.

This simple procedure will form the basis for subsequent more complex procedures described further below. The continuity relationships in step (5) are easily computed. For example; $\dot{m}_{a,\text{out}} = \dot{m}_{a,\text{in}} + \dot{s}_{O_2}$ and $\dot{m}_{f,\text{out}} = \dot{m}_{f,\text{in}} + \dot{s}_{H_2} + \dot{s}_{H_2O}$ while the mass fraction equations are just $m_{k,\text{out}} = m_{k,\text{in}} + \dot{s}_k/(\dot{s}_k + \dot{m}_{k,\text{in}})$, where $k = O_2, H_2, H_2O$, as appropriate.

One important note regards the requirement of prescribed current vs. prescribed voltage. Traditionally physicists work with prescribed voltage, and electrochemists with prescribed current, i (or current density, i''). If it is required that the galvanostatic condition, as opposed to the potentiostatic condition, be prescribed, then it is necessary to adjust the prescribed voltage until the required current is obtained. This is straightforward and two methods for achieving the same end are discussed in Section 2.7.

2 Computer schemes

The numerical scheme described above is of limited practical utility, though it does set the stage for what follows. Numerical schemes vary from very simple schemes requiring a few seconds to run on a personal computer, to complex models which require large computers and long run times. The latter might be used for detailed cell design whereas the former could be employed in a system model including balance-of-plant or for real-time control.

If a SOFC or stack is well-designed, the inlet flow streams will be uniform. However, there may be very substantial variations of mass fraction, temperature, and current density across the fuel cell. Also the flow velocities along the cell passages vary due to mass sources/sinks, and as a result, the pressure may also change in a non-linear fashion. Thus there are many circumstances where it is necessary to solve only the continuity and scalar transport equations, employing the previously-described algorithm, and not involve the pressure-corrected momentum equations in the solution. In other situations, for example when investigating a particular configuration of flow channels, solutions to the momentum equations are required.

It is important to distinguish between situations where the domain is tessellated so finely that diffusive components (viscous effects, heat conduction, and gas diffusion) are captured, and situations where it is necessary to invoke a *rate equation* for the diffusion flux of some general field variable, Φ.

$$-\Gamma \left.\frac{\partial \Phi}{\partial y}\right|_w = g\,\Delta\Phi. \tag{46}$$

The local gradient of Φ at the wall is thus replaced by the bulk-to-wall (or in some cases bulk-to-bulk) difference, $\Delta\Phi$, thus invoking the concept of a *conductance*, g, discussed in detail above in Section 1.6. This notion is central to the classical subject of convective heat and mass transfer [36].

In general, when discretising a SOFC, a mesh will be constructed. It may be structured or unstructured, and it may or may not be boundary fitted (so that each cell corresponds to a given fluid/solid material). For detailed simulations where the diffusion terms are evaluated directly, a fine mesh, concentrated in the near-wall fluid boundaries, will be required as shown in Fig. 10(a). If a rate-equation assumption is invoked, a coarse body-fitted mesh, (b), may be employed, or (c) the mesh may be arbitrary corresponding to local volume averaging. In this case no

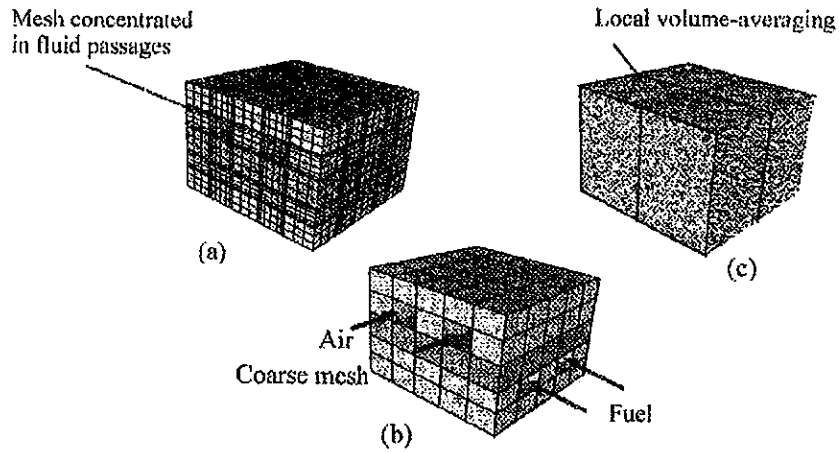

Figure 10: Some possible grids used to discretise a planar SOFC (a) Detailed boundary-fitted (b) Boundary-fitted rate-based formulation (c) Volume-averaged (non-boundary-fitted).

spatial distinction is made between the different materials in the fuel cell. All of these schemes have their advantages and disadvantages. For the latter case storage allocation may be required for more than one phase at each computational cell, whereas for case (b) it is necessary to keep track of all material properties and inter-phase coefficients (conductances), which may be numerous. For case (a), the grid may be so large as to render calculations intractable for large SOFC stacks. Thus there is a trade-off between detail and speed. The code designer is obliged to make some decisions at the outset regarding the nature of the mesh and the corresponding numerical scheme.

Let it be supposed that the SOFC is composed of four distinct media: (1) air, (2) fuel, (3) electrolyte, and (4) interconnect. Let it further be assumed that the electrodes are sufficiently thin that they may be considered as forming the electrolyte surfaces. We shall relax these assumptions in due course. In the next section, we shall consider how to solve such a system using a finite-volume procedure [37].

2.1 General scalar equation

Let is be proposed that a prototype equation having the form

$$\frac{\partial(\rho_j \varepsilon_j \Phi_j)}{\partial t} + \nabla \cdot \left(\rho \varepsilon_j \vec{u}_j \Phi_j\right) = \varepsilon_j \sum_j \alpha_{jk}(\Phi_k - \Phi_j) + \nabla \cdot (\varepsilon_j \Gamma \nabla \Phi_j) + \varepsilon_j \dot{s}''' \quad (47)$$

(i) (ii) (iii) (iv) (v)

be adopted, where Φ is a generic scalar (continuity, mass fraction, enthalpy, etc.) α is a volumetric inter-phase transfer coefficient and Γ is an exchange coefficient. Let the terms in eqn (47) be referred to as, from left to right: (i) *transient*, (ii) *convection*, (iii) *inter-phase transfer*, (iv) *diffusion or within phase transfer*, and (v) *source*.

If the volume fractions, ε_j, are constant they make no contribution to the overall balance, and can be eliminated prior to integrating the equations. Moreover, if a boundary-fitted mesh is employed, $\varepsilon_j = 0$ for all but one 'phase' for which $\varepsilon_j = 1$. For simplicity they will therefore be removed in the analysis. Generally-speaking, terms (iii) and (iv) are mutually exclusive. Also, although (iii) is listed here as a distinct term, it is almost always coded in the form of a linearised source term (v). For steady co-flow, counter-flow and cross-flow, the equations simplify further and in some situations, reduce to ordinary differential equations.

Equation (47) may readily be converted to linear algebraic equations having the form,

$$a_W(\Phi_W - \Phi_P) + a_E(\Phi_E - \Phi_P) + a_S(\Phi_S - \Phi_P) + a_N(\Phi_N - \Phi_P) + \sum C_P(V_P - \Phi_P) + S_P = 0, \tag{48}$$

where in the interests of brevity, the steady 2-D form has been adopted. Equation (48) is the form appropriate to the finite-volume method. The compass notation E = East, W = West, S = South, N = North, T = Previous time step, etc. has been adopted [37]. The terms S_P and $C_P(V_P - \Phi_P)$ are referred to as fixed source and linearised source terms, respectively.

2.2 Continuity

It is usual to solve the phase continuity equations

$$\frac{\partial \rho_j}{\partial t} + \vec{\nabla} \cdot (\rho_j \vec{u}_j) = \dot{m}_j'''. \tag{49}$$

The source terms in the air and fuel passages are due to the electrochemical reactions at the electrodes, namely:

$$\dot{m}_j'' = \pm \sum_k M_k i''/1000nF, \tag{50}$$

where M_k is the molecular weight of chemical element k (O_2, H_2, H_2O) in fluid j, (air or fuel). Since the continuum equations are integrated, it is equivalent to prescribe source terms as being per unit volume or per unit area.

2.3 Momentum

The decision to solve the momentum equations depends on the problem at hand. For single SOFCs where it is known, *a priori*, that the inlet flows are uniform

and steady, there is little point to adding additional complexity to the code. For a 3-D SOFC stack problem, or for a single cell which has yet to be designed, the flow may vary substantially, and it is therefore necessary to solve a generic equation of the form:

$$\frac{\partial(\rho_j \vec{u}_j)}{\partial t} + \vec{\nabla} \cdot (\rho_j \vec{u}_j; \vec{u}_j) = -\vec{\nabla} P_j - F_j \varepsilon_j \vec{u}_j + \vec{\nabla} \cdot (\mu \vec{\nabla} \vec{u}_j), \tag{51}$$

where the subscript j refers to either air or fuel as distinct phases. Since the phases do not intermingle, the inter-phase terms are of the form $F_j \varepsilon_j (0 - \vec{u}_j)$. The second term on the right-side of eqn (51) is normally absent for a detailed numerical analysis, Fig. 10(a). Conversely, for cases Figs 10(b) and (c), it is assumed that if transient and inertial effects were negligible, the overall pressure drop would be entirely due to fluid drag or resistance,

$$\vec{\nabla} P_j = -F_j \vec{U}_j = -\varepsilon_j F_j \vec{u}_j, \tag{52}$$

where $\vec{U}$ is a local *bulk superficial* velocity, $\vec{u}$ is a local *bulk interstitial* velocity, and the quantity F_j has been referred to as a 'distributed resistance'[38], which for a homogeneous porous media of permeability, k_{Darcy}, has the significance

$$F_j = \mu / k_{\text{Darcy}}. \tag{53}$$

Generally-speaking the dependent variable for case Fig. 10(a) is the actual local velocity, $\vec{u}$; for (b) $\vec{u}$ is the local bulk interstitial velocity, and for (c) it may be chosen to be either $\vec{u}$ or $\vec{U}$. For fully-developed laminar duct flows with negligible mass transfer,

$$f^* = \frac{\tau_w}{\frac{1}{2}\rho u^2} = \frac{C}{Re}. \tag{54}$$

Shah and London [35] suggest that for rectangular ducts, dimensions $L \times H$:

$$C = 24(1 - 1.3553\alpha^* + 1.9467\alpha^{*2} - 1.7012\alpha^{*3} + 0.9564\alpha^{*4} - 0.2537\alpha^{*5}), \tag{55}$$

where $\alpha^* = H/L$ or L/H, whichever is a minimum. The Reynolds number, $Re = D_h \rho u / \mu$, is based on a hydraulic diameter $D_h = 4A/P$, where A is the flow area and P is the wetted perimeter. It can readily be shown that

$$F_j = \frac{2C}{\varepsilon} \frac{\mu}{D_h^2}. \tag{56}$$

For a detailed numerical simulation, Fig. 10(a), knowledge of eqns (52) to (56) is irrelevant. The drag is directly obtained from the viscous term in eqn (51). Conversely, for a rate-based formulation, the viscous term is discarded in favour of eqns (52) to (56). In reality, F will also vary due to mass transfer effects, $f/f^* \neq 1$, as $\tau = \mu |\partial u / \partial y|$ is a function of the shape of the velocity profile which depends on the rate of mass transfer. This profile is not necessarily similar to the scalar mass fraction profile [39]; eqn (43) or Fig. 7 cannot be used to correct F. Detailed experimental

or numerical data of f/f^* as a function of the momentum blowing parameter are required for the particular geometry under consideration. At present, this consideration is often simply ignored. Reference [18] contains a comparison of a distributed resistance formulation with a detailed CFD methodology for a SOFC stack including heat and mass transfer effects.

2.4 Heat transfer

Equation (47) is considered appropriate for the analysis of heat transfer, with the solved-for variable generally being written in terms of temperature (not enthalpy or internal energy) as

$$\frac{\partial(\rho_j c_j T_j)}{\partial t} + \vec{\nabla}\cdot(\rho c_j \vec{u}_j T_j) = \sum_j \alpha_{jk}(T_k - T_j) + \vec{\nabla}\cdot(k\vec{\nabla}T_j) + \vec{\nabla}\cdot\vec{q}'' + \dot{q}'''. \quad (57)$$

A volumetric heat source occurs in the electrolyte due to irreversible Joule heating. This is given by

$$\dot{q}''' = \frac{i''(E-V)}{H_e}, \quad (58)$$

where H_e is the thickness of the electrolyte. For thin electrodes the energy of activation at the electrodes may be prescribed as per unit area with a magnitude

$$\dot{q}'' = i''\eta \quad (59)$$

normal to the electrode surface. An additional heat source is due to the entropy change as discussed in Section 1.3 and can be expressed as

$$\dot{q}'' = \frac{i''}{2F}(\Delta G^0 - \Delta H^0). \quad (60)$$

Technically this should be split into anodic and cathodic components. For SOFCs this source term is usually prescribed at the anode. Convective sources exist also by virtue of mass transfer at the walls and these must also be accounted for (see below). The reader will note that there is inter-phase heat transfer between solids and fluids. At the same time there is within-phase metallic conduction, for example in the metallic interconnects. This is one case where both terms (iii) or (iv) in eqn (47) are present. The volumetric heat transfer coefficients are computed as

$$\alpha V = \bar{U}A, \quad (61)$$

where A is the area for heat transfer, V is cell volume, and $\bar{U}$ is an overall heat transfer coefficient, obtained using harmonic averaging, for example;

$$\frac{1}{\bar{U}A} = \frac{1}{hA} + \frac{H}{kAS_{\text{cond}}}, \quad (62)$$

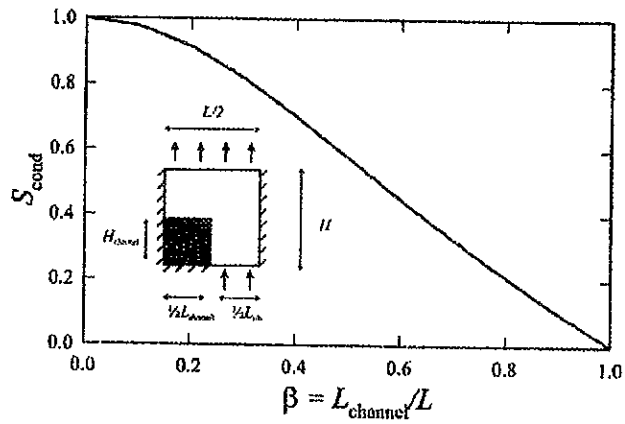

Figure 11: Shape factor for square ducts for the case, $L/H = L_{\text{channel}}/H_{\text{channel}} = 2$.

where S_{cond} is a conduction shape factor. (N.B. the standard definition in heat transfer texts includes the term H/A, where A is the maximum surface area for heat transfer and H is the thickness of the solid region). Figure 11 shows an example of S_{cond} for square geometry. These data were obtained by the present author by means of numerical simulation. The fuel cell designer should obtain S_{cond} from a numerical simulation for the Laplacian system, $\nabla^2\phi = 0$, for the actual geometry under consideration. Fin theory may be employed, if there are significant temperature variations within the interconnects. Conduction shape factors may also be used when considering the potential distribution in the interconnects where the electric resistance is given by

$$r = \frac{H}{\sigma A S_{\text{cond}}}. \tag{63}$$

It is to be noted that for both electric and thermal conduction, the shape function will vary as a function of the direction of the local current density or heat flux vector. It is thus an engineering approximation.

Temperature variations in fuel cells are inevitable, even when the heat sources are entirely uniform (corresponding to uniform current density and resistance). Figure 12 shows typical simulated temperature variations for a cross-flow SOFC; Achenbach [10] compares the performance for co-flow and counter-flow as well. Temperature variations impact in a number of ways; in particular the electrolyte resistance, r_e, is extremely temperature dependent. This in turn influences the current density and hence the internal power dissipation. Temperature also affects the local Nernst potential, E_0. Generally speaking lower temperatures are required for mechanical stability, however if methane is used as fuel, higher temperatures are needed to assist the reforming reaction. The thermally conducting interconnect is beneficial; were it not present, the temperature gradients in Fig. 12 would be much greater.

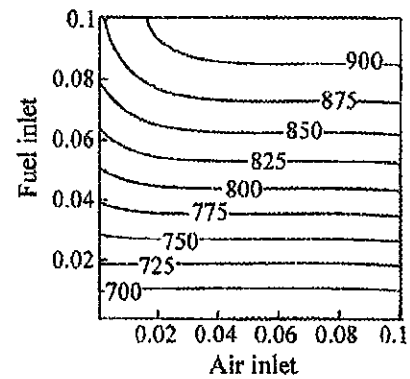

Figure 12: Temperature variation, deg. C, in a SOFC for cross-flow.

2.5 Mass transfer

Treatment for mass transfer within the gas phases is particularly simple, namely:

$$\frac{\partial(\rho m_k)}{\partial t} + \vec{\nabla}\cdot(\rho\vec{u}_j m_k) = \nabla\cdot(\Gamma\nabla m_k) + \vec{\nabla}\cdot\vec{j}_k''', \tag{64}$$

where the diffusion term is absent for cases Fig. 10(b)(c). The reader will note that there are no inter-phase mass transfer terms. Mass sources/sinks at the wall are of the form

$$j_k'' = \dot{m}'' m_{k,s}. \tag{65}$$

Thus mass transfer values are just the T-state values. The wall values, needed for the Nernst equation, are obtained directly by the calculation procedure, for case Fig. 10(a). For cases Fig. 10(b) and (c) these must be computed using eqns (42)–(43), or equivalent, from the local bulk mass fractions. This is particularly simple with the mass-based formulation, given above.

2.6 Numerical integration schemes

The generalised coupled system of equations is quite complex, and we shall illustrate by considering the simplified case of the energy equation for the case of steady 2-D cross-flow, for which numerous terms may be eliminated. Specifically, in the fluids the inter-phase terms (Fig. 10(a)), and/or diffusion terms (Figs 10(b) and (c)) are absent or negligible; in the solids terms (i) and (ii) are absent. Thus we can write eqn (47) for the air and electrolyte in the following reduced forms,

$$(\rho uc)_a\frac{dT_a}{dx} = \alpha_{ae}(T_e - T_a) + \alpha_{ai}(T_i - T_a), \tag{66}$$

$$0 = \vec{\nabla}\cdot k_e\vec{\nabla}T_e + \alpha_{ae}(T_a - T_e) + \alpha_{fe}(T_f - T_e) + \dot{q}''', \tag{67}$$

where the subscripts a, f, e, i refer to air, fuel, electrolyte, and interconnect phases. Similar expressions may easily be written for the fuel and interconnect. These may readily be discretised as follows:

$$\dot{c}_a(T_{aW} - T_{aP}) + \alpha_{ae}V(T_{eP} - T_{aP}) + \alpha_{ai}V(T_{fP} - T_{aP}) + a_F(T^*_{aP} - T_{aP}) = 0, \tag{68}$$

$$d_{ew}(T_{eW} - T_{eP}) + d_{ee}(T_{eE} - T_{eP}) + d_{es}(T_{eS} - T_{eP}) + d_{en}(T_{eN} - T_{eP}) + \alpha_{ae}V(T_{aP} - T_{eP}) + \alpha_{fe}V(T_{fP} - T_{eP}) + a_F(T^*_{eP} - T_{eP}) + \dot{q}_P = 0, \tag{69}$$

where $\dot{c} = \dot{m}c = \rho u \Delta A c$ and $d_e = k\Delta A/|P - E|$ etc., are convection and diffusion terms, respectively. This is a set of simplified 2-D finite-volume equations (eqn (48)) with $\Phi = T$. For air: convection dominates and the linear coefficients are $a_W = \dot{c}_a$, $a_E = a_S = a_N = 0$; the inter-phase terms may be linearised with coefficients $C_e = \alpha_{ae}V$, $C_i = \alpha_{ai}V$, and values $V_e = T_{eP}$, $V_i = T_{iP}$, and there are no internal sources of heat $S = 0$. For the electrolyte: the linkages are diffusive, $a_E = d_{ew}$, etc., and the inter-phase terms are as above, namely $C_a = \alpha_{ae}V$, $C_f = \alpha_{fe}V$, and $V_a = T_{aP}$, $V_f = t_{fP}$. This time, however, there is a heat source $S = \dot{Q}_P$. Thus by careful consideration of the governing equations, it is possible to effect great savings in computer resources, when generating source code in-house. The symbol T^*_P denotes the value of T_P at the previous iteration, and a_F is an inertial or false time step coefficient. This mechanism is used to relax the scheme in order to procure convergence.

2.7 Iterative procedure

The calculation proceeds precisely as in Section 1.7, except that calculations are performed on a per-unit-cell basis rather than at the mean of the inlet and outlet values. A local Nernst potential may be computed:

$$E(x, y) = V + i''r + \eta_a + \eta_c = V + r_i i'', \tag{70}$$

where r_i is a local internal resistance. Average values of Nernst potential, $\bar{E}$, current density, $\bar{i}''$, electrolyte resistance, $\bar{r}_e$ etc. are obtained by summation.

The galvanostatic (constant current) condition is usually implemented for stack models to ensure overall charge conservation. When the overall current or mean current density, $\bar{i}''$, is prescribed, some form of 'voltage correction', V', is required. For example a correction may be applied in the form

$$V' = -r_i\bar{i}', \tag{71}$$

where $V = V^* + V'$ is the desired cell voltage, and V^* is the value of V at the previous iteration; similarly $\bar{i}'' = \bar{i}' + \bar{i}''^*$ is the desired value and $\bar{i}''^*$ is the previous computed value. Thus the mean current density, $\bar{i}''^*$, is computed at the end of each iterative cycle compared to the desired value $\bar{i}$, and the voltage is corrected

accordingly. $\bar{r}_i$ need not be exact; any reasonable value will procure conversion. An alternative approach taken in many codes is to directly set

$$V = \bar{E} - \bar{r}_i \bar{i}''. \tag{72}$$

If eqn (72) is employed, $\bar{r}_i$ must be carefully computed using numerical integration over the surface of the SOFC. Because very small changes in V can effect large changes in i'', relaxation is generally employed. We have used both eqns (71) and (72) with success in our numerical codes and schemes. The reader will note that if the full potential field is solved-for as a scalar variable, as discussed below in Section 2.10, there is no need to adjust the voltage. Another adjustment often made while performing fuel cell calculations is to change the inlet flow rates until particular values of the utilisation for fuel and air are obtained. This is straightforward.

2.8 Additional chemistry and electrochemistry

One advantage of the SOFC is that CO and CH_4 may be used as fuels in addition to pure H_2. This introduces additional kinetics and further complicates mass transfer calculations. If CO is employed as fuel, the anode surface reaction is

$$CO + O^{2-} \rightarrow CO_2 + 2e^-. \tag{73}$$

If both CO and H_2 are present, the two reactions at the anode are considered to be in parallel, but the net anode and cathode reactions are in series, so that

$$i'' = i''_{O_2} = i''_{H_2} + i''_{CO}. \tag{74}$$

The Nernst potentials are not the same, $E_{CO/O_2} \neq E_{H_2/O_2}$, however charge transfer (activation) and mass transfer mechanisms will ensure that the two parallel reaction rates (i''_{H_2} and i''_{CO}) adjust until a single cell potential, V, is obtained, such that

$$V = E_{CO/O_2} - \eta_{CO,a} - \eta_c - i''R = E_{H_2/O_2} - \eta_{H_2,a} - \eta_c - i''R, \tag{75}$$

where $\eta_{CO,a}$ and $\eta_{H_2,a}$ are evaluated iteratively so that $E_{CO/O_2} - \eta_{CO,a} = E_{H_2/O_2} - \eta_{H_2,a}$ where $\eta_{CO,a}$ is a function of i''_{CO}, and $\eta_{H_2,a}$ is a function of i''_{H_2} such that eqn (74) is identically satisfied. Although this adds complexity, nothing fundamental has changed in the basic algorithm. No further assumption need be made regarding the reaction kinetics, other than estimates for i''_0 and β for each anodic reaction, as discussed in Section 1.5.

The CO and H_2 may be produced by reforming methane

$$CH_4 + H_2O \rightarrow CO + 3H_2. \tag{76}$$

The rate of reaction is considered to be kinetically controlled [10]. The water-gas shift-reaction is

$$H_2O + CO \rightarrow CO_2 + H_2. \tag{77}$$

This process is generally considered to be thermodynamically controlled.

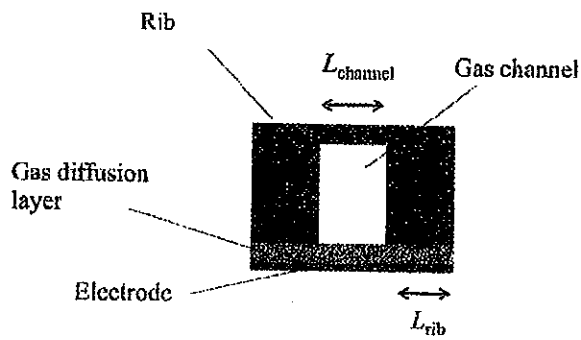

Figure 13: Detail of gas diffusion layer.

2.9 Porous media flow

Up to the present point, the electrodes have been assumed to be sufficiently thin as to be treated as 2-D objects. There are many situations where this is not true, and these should be treated as electro-chemically reacting porous media. Moreover, SOFCs are usually designed with gas diffusion layers, in the form of porous media, as illustrated in Fig. 13. $L_{channel}$ and L_{rib} are the length of the gas channel and the solid 'rib'. Under the circumstances, Darcy's law may be used to compute the flow field, as detailed in Section 2.3. Here is a situation where the volume fraction, ε, should be retained in eqn (47). Reynolds number based on a pore diameter is used to evaluate whether the Forcheimer-modified form [40] is required to account for inertial effects. Many codes compute within-phase mass transfer by assuming an effective diffusion coefficient

$$\Gamma_{eff} = \frac{\Gamma}{\tau}, \tag{78}$$

where τ is a 'tortuosity' factor, which is a measure of the mean interstitial path length of the flow lanes per unit overall length. In general, it is to be noted that the rib design of SOFCs is one of competing interests [41]: a high ratio of $L_{channel}/L_{rib}$, will increase Ohmic losses in the narrow ribs, whereas a low aspect ratio may result in non-uniform concentrations along the widely spaced gas diffusion layer. This is, of course, a function of the diffusivity (and permeability) of the gas diffusion layer as well as the current density.

Recent work [34] has shown that the analysis developed in Section 1.6 may be extended to the combined or conjugate problem of simultaneous mass transfer in both the channels and diffusion layers, provided the driving force, b, is based on the overall or average conductance for the entire geometry, $\bar{g}^*$, obtained by harmonic averaging of the combined conductances of the gas channel and diffusion layer. The relative magnitude of mass transfer in the channels and diffusion layers is determined not only by the values Sh for the gas channel and diffusion layer, but also by the ratio Γ_{eff}/Γ.

It is to be noted that within the electrodes the mean bulk mass fractions must differ from the mean wall values for a current to flow. Since it is not feasible to discretise the actual porous matrix for any practical geometry, the rate of mass transfer will need to be estimated, again using the methodology outlined in Section 1.6, in order that the Nernst equation be correctly prescribed. This will in general require knowledge of Sh^*, for the particular porous media employed. Such data are rarely available. However bulk-to-wall mass transfer will be important at high current densities when the so-called 'diffusion limit' is reached, and should therefore be considered in future codes and methodologies.

Heat transfer in porous media is often analyzed by assuming thermal equilibrium between the two phases, with algebraic averaging employed to compute an effective thermal conductivity

$$k_{\text{eff}} = \varepsilon k_g + (1 - \varepsilon) k_s, \tag{79}$$

where k_g and k_s are the gas-phase and solid-phase conductivities of the medium. When modeling fluid flow, heat and mass transfer in porous media, certain closure assumptions are made by virtue of the local volume-averaging procedure. These closures are quite reasonable and may be considered reliable. The question remains: is it possible to lump the analyses to develop a simpler, less computationally complex model? The answer would appear to be in the affirmative: certainly the techniques applied to heat and mass transfer predictions may readily be applied to the electric field, with volumetric sources and sinks of potential being applied across phase boundaries. Moreover, mass transfer in gas diffusion layers may be amenable to closed form analytic solutions.

2.10 Current and voltage distribution

For planar geometries it is generally sufficient to compute the potential field using the Nernst equation (eqn (20)). This is a local 1-D model. Moreover it is often sufficient to neglect Ohmic losses in the metallic interconnects. We shall now relax these assumptions. The Nernst potential may be considered to be the sum of the potential differences across the anode and cathode, $E = \Delta\phi_a + \Delta\phi_c$, where

$$\Delta\phi_a = \Delta\phi_a^0 + \frac{RT_f}{2F}\left(\ln x_{\text{H}_2} - \ln x_{\text{H}_2\text{O}}\right) - \eta_a, \tag{80}$$

$$\Delta\phi_c = \Delta\phi_c^0 - \frac{RT_a}{4F}\left(\ln P_a + \ln x_{\text{O}_2}\right) - \eta_c, \tag{81}$$

where T_f and T_a are the fuel-side and air-side temperatures (not necessarily the same). As has been discussed, there is an element of arbitrariness in the choice of $\Delta\phi_a^0$ and $\Delta\phi_c^0$.

A number of codes now involve the solution of the Poisson equations for the electric field over the entire region (both ionic and electronic)

$$\vec{\nabla} \cdot (\sigma \vec{\nabla}\phi) = \dot{s}''', \tag{82}$$

where σ is the ionic conductivity in the electrolyte or the electronic conductivity in the interconnects. Equation (82) is to be considered a statement of the principle of conservation of charge, $\vec{i}'' = -\sigma\vec{\nabla}\phi$. This is a simplified version of the scalar equation, eqn (47), and presents no difficulty.

If the electrodes are sufficiently thin, source terms prescribed according to eqn (80) and (81) account for step changes in potential across the anode and cathode. These may be applied as sources of equal and opposite magnitude on either side of the electrode boundary (a 'planar' dipole). Elsewhere in the interconnect and the electrolyte $\dot{s}'''$ is zero, i.e., the Poisson system reduces to Laplace's equation. Since this is a conjugate diffusion problem, harmonic averaging of the conductance, σ, should be employed. When the electrodes are of finite thickness, some care is required as electronic and ionic conduction zones overlap. Under the circumstances, storage is generally assigned for two different scalar potentials. The principle of superposition can be applied to the electric field potential, and other definitions of potential may be encountered.

A variety of external boundary conditions may be applied to obtain the solution for the electric field potential. For example, (i) two voltages, V_1, and V_2 may be applied at the boundaries of the interconnects (Dirichlet problem), alternatively (ii) a uniform current density may be prescribed at both boundaries (Von Neumann problem), with a single point within the assembly fixed to a reference potential, or (iii) the current density may be fixed at one interconnect and the voltage at the other (mixed boundary value problem).

Figure 14 shows flux lines of current density computed from the electric potential. In this case the field is quite uniform, though in situations where mass fractions of the products/reactants vary substantially at high i'', the iso-galvanic lines can be highly non-uniform. The additional effort required to obtain a solution for the electric potential should only be undertaken if significant non-uniformities in the current distribution are anticipated. This approach is generally combined with an analysis of flow and mass transfer in the porous gas diffusion layers on either side of the electrodes.

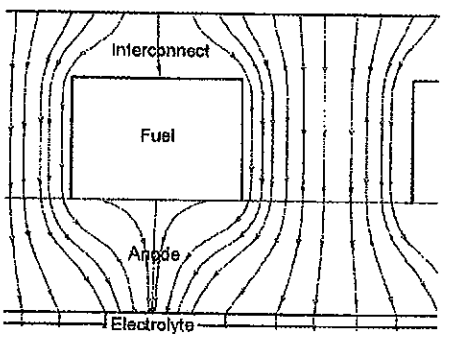

Figure 14: Particle traces along galvanostatic lines. From [34].

It is worthy of note that the Poisson system, eqn (82), can be considered to be a simplified version of the Nernst-Planck equation,

$$\vec{i}'' = \frac{2F}{M}(\rho\vec{u} - \Gamma\vec{\nabla}m) - (\sigma\vec{\nabla}\phi), \tag{83}$$

where for convenience we assume the presence of only a single charge carrier, O^{2-}, in the electrolyte. Diffusion and convection are generally considered subordinate to migration in the SOFC electrolyte.

2.11 Advanced diffusion models

The development derived in Section 1.6 is appropriate to so-called 'ordinary' diffusion, for which the diffusion flux is given by Fick's law:

$$\vec{j}'' = -\rho D\vec{\nabla}m. \tag{84}$$

Such an analysis is appropriate [42] for non-dilute, multi-component mixtures only if

$$D_{12} = D_{13} = \cdots D_{jk} = D = \frac{\Gamma}{\rho}. \tag{85}$$

Kays *et al.* [31] suggest that this is indeed approximately the case for high temperature gases, as occur in SOFCs. If it is not the case, the simplest procedure is to calculate an effective diffusion component according to Wilkes [43] as

$$D_{k,\text{eff}} = \frac{1 - x_k}{\sum_{j\neq k}\frac{x_j}{D_{jk}}} \tag{86}$$

which is exact, only for dilute mixtures in a concentrated carrier fluid. A more complete analysis involves the solution of the Stefan-Maxwell equations [44] for the diffusion fluxes

$$\vec{\nabla}(m_k M) = \frac{M^2}{\rho}\sum_{j=1}^{n}\frac{m_k\vec{j}_j - m_j\vec{j}_k}{M_j D_{jk}}. \tag{87}$$

The set of eqns (87) may be regarded as implicit expressions for the diffusion fluxes, $\vec{j}_k$. These may then be substituted into eqn (64) in the usual fashion, to obtain the mass fractions, m_k. Typically, the linear coefficients in the finite-volume equation (eqn (48)) are caste in the same form as for 'ordinary' diffusion and an additional source term added [45]. This has the effect of preserving the correct form of non-linearity in the transport equations, for the case of binary diffusion. If the pore size is sufficiently small that it approaches the mean free path of the colliding particles, *Knudsen diffusion* must also be considered. Finally *surface diffusion* may also occur. Multi-component diffusion in reacting porous media is a highly complex subject, considered beyond the scope of this brief introduction.

2.12 Thermal radiation

A SOFC is a high temperature device, and even though temperature differences within the passages may be small, they may nonetheless be such that radiative heat transfer is present. The relative importance of radiation in SOFCs is currently the subject of debate. Radiation may be important within the gas channels, within the electrolyte-electrode assembly, and also when thermal insulation layers are employed. Reference [46] reviews some of these issues.

Surface-to-surface radiation in the micro-channels may be accounted-for by the network method [47],

$$\dot{q}_k = \frac{\sigma T_k^4 - q_{0k}}{(1-\varepsilon_k)/\varepsilon_k A_k} = \sum_{j=1}^{N} \frac{q_{0j} - q_{0k}}{1/F_{k-j}A_k}, \tag{88}$$

where ε_k and A_k are the emissivity and area of the kth element, q_{0k} is the radiosity (the total of emitted and reflected radiation), F_{k-j} is a configuration factor [48], and $\sigma = 5.67 \times 10^{-8}\,\mathrm{W \cdot m^2 K^4}$ is the Stefan-Boltzmann constant. The terms $(1-\varepsilon_k)/\varepsilon_k A_k$ and $1/F_{k-j}A_k$ in the denominators are referred to as 'surface' and 'space' resistances respectively. By the construction a network of resistances, the unknown radiosities may be eliminated and the system of equations solved. Since the micro-channels are very narrow, only a few immediate neighbours (opposite and sides) in any given channel will be of any consequence, and the computation can then be much simplified. The additional work involved in computing surface-to-surface radiation along the length of the channel is probably not justified. Yakabe *et al.* [49] describe a procedure for calculating surface-to-surface radiation in gas micro-channels, which differed from the standard analysis, eqn (88). VanderSteen *et al.* [50] suggest that surface-to-surface radiation could affect the temperature by as much as 25–50 K.

Although the gas channels are amenable to a simplified analysis, the electrolyte, and possibly the electrodes of a SOFC constitute radiatively participating media. Murthy and Fedorov [51] suggest the exclusion of radiation effects in the participating electrolyte could result in the over-prediction of temperatures by as much as 100–200K for the case of an electrolyte-supported SOFC. By contrast, refs. [52, 53] suggest very modest differences in electrolyte temperature; less than 1 K. These disparities indicate that the need to include radiation effects is, at present, still a moot point. Reference [51] suggests that the electrolyte may be treated as being optically thin, while the electrodes may be considered as optically thick. A very limited amount of experimental data has been gathered in support of this, to date; however [52, 53] suggest that in fact, the electrodes are so optically thick as to be entirely opaque for all practical purposes.

The general radiation heat transfer problem in a participating medium involves heat transfer 'at a distance'; described mathematically by an integro-differential equation, referred to as the *radiative transfer equation* (RTE). For a grey

isotropically-scattering medium, this may be written in the simplified form,

$$\frac{di}{ds} = -(a+\sigma_s)\,i + a\frac{e_b}{\pi} + \frac{\sigma_s}{4\pi}\int_{\omega=0}^{4\pi} i\,d\omega. \tag{89}$$

(i) (ii) (iii) (iv)

In this section only, the symbol i denotes radiant intensity (not electrical current), a and σ_s are absorption and scattering coefficients, s is displacement, ω is solid angle, and $e_b = \sigma T^4$ is black-body emissive power. The terms in eqn (89) represent (i) changes in intensity, i, due to: (ii) absorption and out-scattering, (iii) emission, and (iv) in-scattering, respectively. Detailed numerical solutions to the RTE are typically conducted using a *discrete ordinate method* or a *Monte Carlo method.* The former is more popular, at the present time, but suffers from 'ray effects' which can lead to numerical errors. The RTE solution results in a field of values for the radiation intensity from which a radiant flux vector, $\vec{q}''$, can be calculated for substitution in the energy equation. However, both the discrete ordinate, and Monte Carlo methods are very compute-intensive. Therefore some additional engineering assumptions are required if it is possible to invoke simpler radiation models within multi-channel fuel cells and stacks.

For *optically thin regions* a multi-flux model may be considered, for which the 1-D *two-flux model* is the simplest. It is referred to, in the literature, as the Schuster-Schwarzschild approximation. If it is assumed that the intensity is composed of two homogeneous components such that $\dot{q}^+ = \pi i^+$ and $\dot{q}^- = \pi i^-$ in the $+x$ and $-x$ directions, then it can readily be shown that eqn (89) may be written as,

$$\frac{d}{dx}\left(\frac{1}{a+\sigma_s}\frac{d\bar{q}}{dx}\right) = 4a\left(\bar{q} - e_b\right), \tag{90}$$

where $\bar{q} = \left(\dot{q}^+ + \dot{q}^-\right)/2$, and for which (the x-component of) the radiant flux vector, $\dot{q}'' = \dot{q}^+ - \dot{q}^-$, may be computed as

$$\dot{q}'' = -\frac{1}{a+\sigma_s}\frac{d\bar{q}}{dx}. \tag{91}$$

Equation (90) is a diffusion-source equation, and is thus suitable for discretisation in the form eqn (48). It has been presented in the form developed by Spalding [54], from which it differs slightly mathematically, being consistent with the formulation in Siegel and Howell [48]. A six-flux model may similarly be constructed in terms of three field variables, $\bar{q}_x$, $\bar{q}_y$, $\bar{q}_z$ in 3-D, and has the advantage of being in the same form as the general scalar equation (eqn (47)). However for thin plane layers, a two-flux model may be sufficient. The discrete ordinate method may be regarded as a generalised multi-flux method [48].

For *optically thick* regions, a *diffusion approximation* is considered appropriate, with radiative conductivity defined by,

$$k_R = \frac{16n^2\sigma T^3}{3a}, \tag{92}$$

a is a (Rosseland mean) absorption coefficient. The term, k_R, may simply be added to the normal conduction term, k, in eqn (57), i.e., $k_{eff} = k + k_R$. There are however difficulties associated with use of the diffusion approximation near boundaries. This may be remedied by the use of a temperature modified slip boundary condition [48].

Thermal radiation is one mechanism by which it may be possible to actually control stack temperature and temperature gradients, by manipulating the optical properties of the component materials or employing radiation shields. Spinnler *et al.* [55, 56] propose the use of highly-reflective thermal insulation to control fuel cell temperatures by minimising losses to the environment.

The above analysis adds considerably to the complexity of the calculation procedure, even so for situations where radiation is important; it is probably over-simplistic: In reality, the electrolyte assembly is a porous media with non-homogeneous optical properties, including dependent scattering, while the interconnect is typically metallic and hence there may be both specular and diffuse components to the surface radiosity. The spectral nature of the radiative properties of the SOFC components also need to be determined. The subject has received little attention to-date and should be considered a topic for future research by scientists and engineers seeking to design high-temperature fuel cells.

The four outstanding technical issues in numerical analysis of themo-fluids are; chemical kinetics multi-phase flow, radiative heat transfer and turbulence. For SOFCs, the chemical kinetics is a complex issue that needs to be addressed; multi-phase flow is superficially not a problem, but the presence of porous media and the need for volume-averaging raises many of the same issues. Thermal radiation may be a matter for concern, as discussed above. Turbulence is not generally generated at the Reynolds numbers encountered within the passages of planar SOFCs, however turbulence may be encountered within the inlets and outlets and manifold passages of SOFC stacks.

3 Stack models

SOFCs are stacked to increase the working voltage to a reasonable value. Fuel and air are typically introduced via manifolds (risers and downcomers). Various design configurations are possible. The main concerns of the stack designer are uniformity of flow and pressure gradients. If SOFCs were not operated in stacks, it probably would be feasible to conduct detailed numerical analysis using CFD codes without invoking a rate equation assumption, at least for simple geometries. The presence of numerous fuel cells, each with multiple channels, renders this situation unlikely for large stacks for the foreseeable future.

A rough estimate of the relative magnitude of parasitic losses in the cells and manifolds can be made by assuming the flow is uniform, then analysing to see if this is a reasonable assumption. It may readily be shown from eqns (54) and (55), that for planar passages neglecting injection/suction that the pressure drop across the stack is just,

$$\Delta \bar{P} = \frac{48 L \mu \bar{u}}{H^2} = \frac{48 L \mu \dot{Q}}{n_{fc} W H^3}, \tag{93}$$

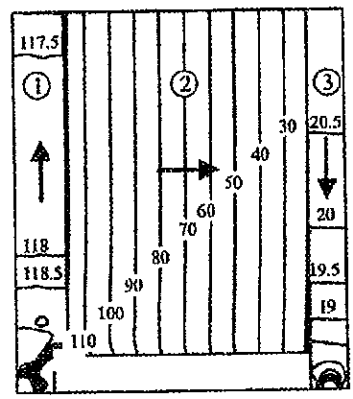

Figure 15: Pressure (Pa) in a 50-cell SOFC stack assembly. From [57].

where n_{fc} is the number of fuel cells in the stack, $2H$ is the height of the (air or fuel) channels, W is the width of the cell, L is the length of the fuel cells in the flow direction, and $\dot{Q} = n_{fc}BH\bar{u}$ is the volumetric discharge, assuming uniform flow conditions. A similar, though more complex, expression may be readily derived for rectangular passages. The basic principle of stack design is that the losses across the cells should be large in comparison to those in the inlet manifolds. Large changes in pressure drop are effected by changing the height of the passages, since $\Delta\bar{p} \propto 1/H^3$.

Equation (93) is to be considered only approximate. Mass transfer will increase or decrease pressure for the cases of injection and suction, respectively. This purely inertial effect is in addition to the frictional f/f^* effects discussed earlier (recall Bernoulli's law $P + \frac{1}{2}\rho u^2 = \text{constant}$). In the manifolds suction/blowing leads to all fluid being entirely evacuated over the stack height, H, and the latter must be considered. Berman [58] was the first to derive an analytical solution for the pressure distribution for a plane duct with mass transfer at both walls; analyses for suction/blowing at only one wall also exist [59, 60]. For rectangular geometry it is simple to utilize a numerical calculation (CFD) procedure. Figure 15 shows the pressure distribution in a 50-cell stack assembly; it can be seen that (1) in the inlet manifold the pressure gradient decreases due to suction, (2) there is relatively uniform pressure within the stack, and (3) an increasing pressure gradient is observed in the outlet manifold due to side-injection. The reader will note that different contour scales have been used in the stack and manifold regions and that the overall (parasitic) pressure losses are much larger in the former than the latter. As the stack height increases, the pressure difference between the manifolds at the top of the stack becomes much less than at the bottom and flow maldistributions may occur.

Another interesting feature of fuel cell stacks is that secondary temperature distributions in the vertical direction arise, even when the flow and heat source term (due to Joule heating) are entirely uniform. Figure 16 shows the temperature distribution in a 10-cell stack obtained using a detailed numerical simulation. The oscillations in the temperature contours are due to the finite differences in temperature between

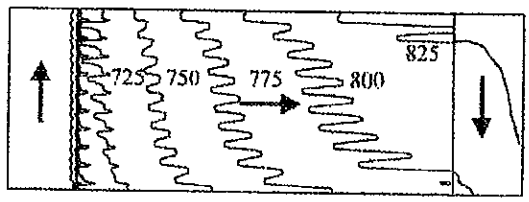

Figure 16: Temperature distribution (deg. C) in a 10-cell SOFC stack with uniform heat sources. Adapted from [34].

the air, fuel, electrolyte and interconnects for each cell in the stack. The secondary temperature gradients are caused by these materials being ordered, creating a net heat flux in the vertical direction. The stack designer cannot necessarily presume that thermo-mechanical behavior is the same for a stack as for a single cell, as has been presumed by many researchers in the past.

4 Closure

Transport phenomena in SOFCs influence every aspect of their design and operation. Fluid flow, heat conduction, convection, and radiation, mass transfer, electrochemistry, charge transfer kinetics and thermodynamics are all important mechanisms. In the last 5–10 years much progress has been made in the development of robust engineering computer codes to model transport phenomena and physico-chemical hydrodynamics in these devices. This is significant progress, however further developments are needed both in models and on input data of properties.

Although it is currently fashionable to state that growth in this area is 'rapid', it remains to be seen whether recent events will continue to be sustainable. On the one hand, design methodologies may continue to evolve exponentially, as the product unfolds and becomes commercially viable in the years to come. On the other, it could be that analysis tools will plateau and languish, if the technology proves to be uncompetitive, and promises of economic viability prove to be a 'bubble'. The author's hope is that the former will prove to be the case, and that years from now, we will see improvements, not only in analysis methods, but also as a result, in the products.

It is clear that if SOFCs, or indeed any other new technologies, are to supplant existing products and processes, they must be designed properly. Every available analysis tool and advanced scientific method needs to be brought to bear upon the problem, if good engineering is to replace good will and sway the public to buy new and untested products over established and functioning ones, in a competitive market place.

In many ways the success or failure of fuel cells will ultimately depend on factors completely unrelated to the thermodynamic efficiency of the electrode-electrolyte assembly, so popular among research proposals. Probably reliability and safety

rank even higher than cost-per-unit energy, and while mathematical modeling alone cannot safeguard these attributes, careful engineering using established techniques such as those described in the chapters in this book (and already widely employed in design of conventional power-generation equipment) will likely prove a good investment, and aid in better understanding of equipment performance. To be competitive, fuel cells need to be at least as well or better designed than existing products.

Finally, for a variety of reasons, numerical models of physico-chemical processes can now be developed in much shorter time-scales (months), and for much less cost than it takes to build complex experimental test rigs (years). While this situation cannot be blamed upon those who seek to construct models and codes, it is nonetheless an unhealthy situation; a balanced program of research should always involve the continuous feedback of experimental data to analysis tools, as well as the abstraction of that which is being modelled to the pragmatist. It is therefore imperative to establish reliable data bases of empirical data for code evaluation purposes.

Acknowledgements

There are many people who have assisted the author in this endeavour, both directly and indirectly. Thanks are due to (in alphabetical order): Katherine Cook, Kyle Daun, Wei Dong, Eliezer Gileadi, Ron Jerome, Yongming Lin, Fengshan Liu, and Rod McMillan.

References

[1] Appleby, A.J. & Foulkes, F.R., *Fuel Cell Handbook*, Van Nostrand Reinhold: New York, 1989.

[2] Kordesh, K. & Simader, G., *Fuel Cells and their Applications*, VCH: New York, 1996.

[3] Larminie, J. & Dicks, A., *Fuel Cell Systems Explained*, Wiley: Chichester, 2000.

[4] Williams, K.R., *An Introduction to Fuel Cells*, Elsevier: Amsterdam, 1966.

[5] Vayenas, C.G. & Hegedus, L.L., Cross-flow, solid-state electrochemical reactors: A steady-state analysis. *Ind. & Eng. Chem. Fundamentals*, **24**, pp. 316–314, 1985.

[6] Fiard, J.M. & Herbin, R., Comparison between finite volume and finite element methods for the numerical simulation of an elliptic problem arising in electrochemical engineering. *Computational Methods in Applied Mechanical Engineering*, **115**, pp. 315–338, 1994.

[7] Ferguson, J.R., Analysis of temperature and current distributions in planar SOFC designs. *Proceedings Second International Symposium on Solid Oxide Fuel Cells*, Athens, Greece, pp. 273–280, 1991.

[8] Herbin, R., Fiard, J.M. & Ferguson, J.R., Three-dimensional numerical simulation of the temperature, potential and concentration distributions of a unit

cell for various geometries of SOFCs. *Proceedings, European Solid Oxide Fuel Cell Forum I*, Luzern, Switzerland, 1994.

[9] Karoliussen, H., Nisancioglu, K., Solheim, A., Odegard, R., Singhal, S.C. & Iwahara, H., Mathematical modeling of cross plane SOFC with internal reforming. *Proceedings, Third International Symposium on Solid Oxide Fuel Cells*, Honolulu, Hawaii, 1993.

[10] Achenbach, E., Three-dimensional modeling and time-dependent simulation of a planar solid oxide fuel cell stack. *Journal of Power Sources*, **73**, pp. 333–348, 1994.

[11] Bessette, N.F. & Wepfer, W.J., Electochemical and thermal simulation of a solid oxide fuel cell. *Chemical Engineering Communications*, **147**, pp. 1–15, 1996.

[12] Bernier, M., Ferguson, J. & Herbin, R., A 3-dimensional planar SOFC stack model. *Proceedings, Third European Solid Oxide Fuel Cell Forum*, Nantes, France, pp. 483–495, 1998.

[13] Ahmed, S., McPheeters, C. & Kumar, R., Thermal-Hydraulic model of a monolithic solid oxide fuel cell. *Journal of the Electrochemical Society*, **138**, pp. 2712–2718, 1991.

[14] Sira, T. & Ostenstad, M., Temperature and flow distributions in planar SOFC stacks. *Third International Symposium on Solid Oxide Fuel Cells*, Honolulu, Hawaii, pp. 851–860, 1993.

[15] Costamagna, P. & Honegger, K., *J. Electrochem. Soc.*, **145(11)**, pp. 2712–2718, 1998.

[16] Chan, S.H., Khor, K.A. & Xia, Z.T., *Journal of Power Sources*, **93**, pp. 130–140, 2001.

[17] Beale, S.B., Lin, Y., Zhubrin, S.V. & Dong, W., Computer Methods for Performance Prediction in Fuel Cells. *Journal of Power Sources*, **11(1–2)**, pp. 79–85, 2003.

[18] Beale, S.B. & Zhubrin, S.V., A distributed resistance analogy for solid oxide fuel cells. *Numerical Heat Transfer, Part B*, in press.

[19] Newman, J.S., *Electrochemical Systems*, Prentice-Hall Inc.: Englewood Cliffs, N.J., 1973.

[20] Levich, V.G., *Physicochemical Hydrodynamics*, Prentice-Hall: Englewood Cliffs, N.J., 1962.

[21] Probstein, R.F., *Physicochemical Hydrodynamics: An Introduction*, Butterworths: Boston, 1989.

[22] Callen, *Thermodynamics*, John Wiley & Sons Inc.: New York, 1960.

[23] Glasstone, S., Laidler, K.J. & Eyring, H., *The Theory of Rate Processes: The Kinetics of Chemical Reactions, Viscosity, Diffusion and Electrochemical Phenomena*. International Chemical Series, McGraw-Hill: New York, 1941.

[24] Gileadi, E., *Electrode Kinetics for Chemists, Chemical Engineers, and Material Scientists*, Wiley-VCH: New York, 1993.

[25] Bockris, J.O.M., Reddy, A.K.N. & Gamboa-Aldeco, M., *Modern Electrochemistry*. Vol. 2, Plenum: New York, 2000.

[26] Bard, A.J. & Faulkner, L.R., *Electrochemical Methods*, 2nd edn, John Wiley & Sons: New York, 2001.
[27] *Fuel Cell Handbook*, 5th edn, U.S. Department of Energy, National Energy Technology Laboratory: Morgantown/Pittsburgh, 2000.
[28] Beale, S.B., Calculation procedure for mass transfer in fuel cells. *Journal of Power Sources*, **128(2)**, pp. 185–192, 2004.
[29] Spalding, D.B., *Convective Mass Transfer: An Introduction*, Edward Arnold: London, 1963.
[30] Spalding, D.B., A standard formulation of the steady convective mass transfer problem. *International Journal of Heat and Mass Transfer*, **1**, pp. 192–207, 1960.
[31] Kays, W.M., Crawford, M.E. & Weigand, B., *Convective Heat and Mass Transfer*, 4th edn, McGraw-Hill: New York, 2005.
[32] Mills, A.F., *Mass Transfer*, Prentice Hall: Upper Saddle River, N.J., 2001.
[33] Kays, W.M. & Crawford, M.E., *Convective Heat and Mass Transfer*, 2nd edn, McGraw-Hill: New York, 1980.
[34] Beale, S.B., Conjugate mass transfer in gas channels and diffusion layers of fuel Cells. *Proceedings 3rd International Conference on Fuel Cell Science, Engineering and Technology*, eds R.K. Shah & S.G Kandlikar, ASME: Ypsilanti, Michigan, 2005.
[35] Shah, R.K. & London, A.L., Laminar flow forced convection in ducts. *Advances in Heat Transfer*, eds T.F. Irvine & J.P. Hartnett, Academic Press: New York, 1978.
[36] Jacob, M., *Heat Transfer*, Wiley: New York, 1949.
[37] Patankar, S.V., *Numerical Heat Transfer and Fluid Flow*, Hemisphere: New York, 1980.
[38] Patankar, S.V. & Spalding, D.B., A Calculation Procedure for the Transient and Steady-state Behavior of Shell-and-tube Heat Exchangers. *Heat Exchangers: Design and Therory Sourcebook*, eds N. Afgan & E.U. Schlünder, Scripta Book Company: Washington, D.C., 1974.
[39] Beale, S.B., Mass transfer in plane and square ducts. *International Journal of Heat and Mass Transfer*, in press.
[40] Vafai, K. & Tien, C.L., Boundary and Inertia Effects on Flow and Heat Transfer in Porous Media. *International Journal of Heat and Mass Transfer*, **24(2)**, pp. 195–203, 1981.
[41] Ferguson, J.R., Fiard, J.M. & Herbin, R., Three-dimensional numerical simulation for various geometries of solid oxide fuel cells. *Journal of Power Sources*, **58**, pp. 109–122, 1996.
[42] Knuth, E.L., Multicomponent diffusion and Fick's law. *Physics of Fluids*, **2**, pp. 339–340, 1959.
[43] Wilke, C.R., Diffusional properties of multicomponent gases. *Chemical Engineering Progress*, **46(2)**, pp. 95–104, 1950.
[44] Taylor, R. & Krishna, R., *Multicomponent Mass Transfer*, Wiley-Interscience: New York, 1993.

[45] Kleijn, C.R., van der Meer, T.H. & Hoogendoorn, C.J., A mathematical model for LPCVD in a single wafer reactor. *Journal of the Electrochemical Society*, **136(11)**, pp. 3423–3433, 1989.
[46] Damm, D.L. & Fedorov, A.G., Radiation heat transfer in SOFC materials and components. *Journal of Power Sources*, in press.
[47] Oppenheim, A.K., Radiation analysis by the network method. *Transactions of the ASME*, **78**, pp. 725–735, 1956.
[48] Siegel, R. & Howell, J.R., *Thermal Radiation Heat Transfer*, 4th edn, Hemisphere: Washington, 2002.
[49] Yakabe, H., Ogiwara, T., Hishinuma, I. & Yasuda, I., 3-D model calculation for planar SOFC. *Journal of Power Sources*, **102**, pp. 144–154, 2001.
[50] VanderSteen, J.D.J., Austin, M.E. & Pharaoh, J.G., The role of radiative heat transfer with participating gases on the temperature distribution in solid oxide fuel cells. *Proceedings 2nd International Conference on Fuel Cell Science, Engineering and Technology*, eds R.K. Shah & S.G. Kandlikar, Rochester, NY, 2004.
[51] Murthy, S. & Federov, A.G., Radiation heat transfer analysis of the monolith type solid oxide fuel cell. *Journal of Power Sources*, **124**, pp. 453–458, 2003.
[52] Damm, D.L. & Fedorov, A.G., Spectral radiative heat transfer of the planar SOFC. *Proceedings International Mechanical Engineering Congress and Exposition*, ASME: Anaheim, California, 2004.
[53] Daun, K., J., Beale, S.B., Liu, G. & Smallwood, G.J., Radiation heat transfer in solid oxide fuel cells. *Proceedings of 2005 Summer Heat Transfer Conference*, ASME: San Francisco, California, 2005.
[54] Spalding, D.B., *Mathematical Modelling of Fluid-mechanics, Heat-transfer and Chemical-reaction Processes: A Lecture Course*, 1980, Computational Fluid Dynamics Unit, Imperial College, University of London: London.
[55] Spinnler, M., Winter, E.R.F. & Viskanta, R., Studies on high-temperature multilayer thermal insulations. *International Journal of Heat and Mass Transfer*, **47**, pp. 1305–1312, 2004.
[56] Spinnler, M., Winter, E.R.F., Viskanta, R. & Sattelmayer, T., Theoretical studies of high-temperature multilayer thermal insulations using radiation scaling. *Journal of Quantitative Spectroscopy and Radiative Transfer*, **84**, pp. 477–491, 2004.
[57] Beale, S.B., Ginolin, A., Jerome, R., Perry, M. & Ghosh, D., Towards a virtual reality prototype for fuel cells. *PHOENICS Journal of Computational Fluid Dynamics and its Applications*, **13(3)**, pp. 287–295, 2000.
[58] Berman, A.S., Laminar flow in channels with porous walls. *Journal of Applied Physics*, **24(9)**, pp. 1232–1235, 1953.
[59] Jorne, J., Mass transfer in laminar flow channel with porous wall. *Journal of the Electrochemical Society*, **129(8)**, pp. 1727–1733, 1982.
[60] Lessner, P. & Newman, J.S., Hydrodynamics and Mass-Transfer in a Porous-Wall Channel. *Journal of The Electrochemical Society*, **131(8)**, pp. 1828–1831, 1984.

Nomenclature

A	Area (m^2)
a	Absorption coefficient (m^{-1}), coefficient in finite-volume equations, length (m)
B	Width (m)
b	Length (m)
c	Specific heat (J/kgK)
D	Diffusion coefficient (m^2/s)
D_h	Hydraulic diameter (m)
E	Nernst potential (V), electric potential (V)
e_b	Black-body emissive power (W/m^2)
F	Distributed resistance (kg/m^2s), Faraday's constant, 96.48 (Coulomb/mol), Radiation configuration factor ()
G	Gibbs free energy (J)
g	Mass transfer conductance (kg/s)
H	Height (m), enthalpy (J)
h	Heat transfer coefficient (W/m^2K), Planck constant 6.626×10^{-34}(J.s)
i	Current (A), radiant intensity ($W/sr.m^2$)
j	Diffusion source
K_P	Equilibrium constant
k	Thermal conductivity (W/mK), rate constant (mol/m^2)
k_{Darcy}	Permeability (m^2)
k	Thermal conductivity (W/mK)
k_r	Radiative conductance (W/mK)
L	Length (m)
M	Molecular weight (kg/mol)
m	Mass fraction (kg/kg), mass (kg)
N	Number of cells in stack (), mole number
n	Charge number (), valence ()
n_{fc}	Number of fuel cells in SOFC stack
P	Pressure (Pa), partial pressure (Pa)
Q	Charge (Coulomb)
$\dot{Q}$	Volumetric discharge (m^3/s)
q	Heat source term (W)
q_0	Radiosity (W)
R	Gas constant, 8.314×10^3 (J/molK), resistance (Ohm)
r	Resistance (Ohm/m^2)
S	Entropy (J/K)
S_{cond}	Conduction shape factor ()
s	Source term, specific heat (J/kgK)
T	Temperature (°C)
U	Internal energy (J), superficial velocity (m/s)
$\bar{U}$	Overall heat transfer coefficient (W/m^2K)

$\vec{u}$	Interstitial velocity (m/s)
V	Volume (m^3), voltage (V)
W	Work (J)
T	Temperature (K)
x_i	Mole fraction (mol/mol)

Greek symbols

α	Volumetric transfer coefficient (W/m^3K)
α^*	Aspect ratio ()
β	Transfer coefficient, symmetry coefficient (), Blockage factor ()
ε	Volume fraction, void fraction (), emmissivity (m^{-1})
Γ	Exchange coefficient (kg/ms)
Φ	General scalar
ϕ	General scalar, electric field potential (V)
η	Overpotential, polarisation (V)
ν	Stoichiometric coefficient
ρ	Density (kg/m^3)
μ	Chemical potential (J/mol), viscosity (W/mK)
σ	Electric conductivity ($Ohm^{-1}m$), Stefan-Boltzmann constant 5.67×10^{-8} (W/m^2K^4)
σ_S	Scattering coefficient (m^{-1})
τ	Shear stress (N/m^2), tortuosity ()

Non-dimensional numbers

B	Driving force
b	Blowing parameter
f	Friction coefficient
Nu	Nusselt number
Sh	Sherwood number
Sc	Schmidt number
Re	Reynolds number

Subscripts

0	Reference state
a	Air, anode
b	Bulk, backward
c	Cathode
e	Electrolyte
f	Fuel, forward
i	Interconnect, internal

l	Load
t	total, transferred substance state
w	Wall

Superscripts

0	Reference state, equilibrium state
*	Zero mass transfer
.	Per unit time
'	Per unit length
+	Positive direction
−	Negative direction

KATHERINE COOK
INFORMATION SPECIALIST
INST FOR CHEM PROCESS & ENVIR TECH
NATIONAL RESEARCH COUNCIL CANADA
MONTREAL ROAD BLDG M12 RM 140
OTTAWA, ON K1A 0R6
CANADA

Client Number:	MCLANCY
Title:	**TRANSPORT PHENOMENA IN FUEL CELLS**
Author:	B. SUNDEN, M. FAGHRI
Date:	2005
Pages:	43–82
Article Title:	SOLID OXIDE FUEL CELLS
Article Author:	S.B. BEALE
Series Title:	DEVELOPMENTS IN HEAT TRANSFER, VOL. 19
Publisher:	WIT PRESS, SOUTHAMPTON, BOSTON

Estimated cost for this 40 page document: $0 document supply fee + $0 copyright = $0